Analysis of Decentralized Control for Absorption Cycle Heat Pumps

Vinther, Kasper; Just Nielsen, Rene; Nielsen, Kirsten Mølgaard; Andersen, Palle; Pedersen, Tom Søndergård; Bendtsen, Jan Dimon

Published in:
Control Conference (ECC), 2015 European

DOI (link to publication from Publisher):
10.1109/ECC.2015.7330871

Publication date:
2015

Document Version
Early version, also known as pre-print

Analysis of Decentralized Control for Absorption Cycle Heat Pumps

Kasper Vinther[1], René J. Nielsen[2], Kirsten M. Nielsen[1], Palle Andersen[1],
Tom S. Pedersen[1] and Jan D. Bendtsen[1]

***Abstract*— This paper investigates decentralized control structures for absorption cycle heat pumps and a dynamic nonlinear model of a single-effect LiBr-water absorption system is used as case study. The model has four controllable inputs, which can be used to stabilize the operation of the heat pump under different load conditions. Different feasible input-output pairings are analyzed by computation of relative gain array matrices and scaled condition numbers, which indicate the best pairing choice and the potential of each input-output set. Further, it is possible to minimize the effect of cross couplings and improve stability with the right pairing of input and output. Simulation of selected candidate input-output pairings demonstrate that decentralized control can provide stable operation of the heat pump.**

I. Introduction

Heat pumps are primarily constructed based on one of two different technologies: vapor compression and absorption. Vapor compression-based heat pumps are predominantly used in domestic and commercial buildings due to their high Coefficient of Performance (COP), whereas absorption-based heat pumps are used in industrial applications where significant amounts of cheap waste heat is available.

The basic absorption cycle works similarly to the vapor compression cycle except that the compressor is replaced by an absorber and a generator, and the working fluid in an absorption refrigeration system is a binary solution consisting of refrigerant and absorbent. In the generator, the refrigerant and absorbent are chemically separated as the refrigerant vaporizes, drawing heat from the surroundings. The refrigerant vapor is then led to a condenser, where a normal condensation occurs, expelling heat to the surroundings. Saturated refrigerant is fed to an evaporator through a valve, where it evaporates, consuming heat from the surroundings. Finally, the vapor is led to an absorber, where concentrated absorbent absorbs refrigerant vapor at low pressure; this absorption process is an exothermic process, which means that it must reject heat to the surroundings. As the separation process occurs at a higher pressure than the absorption process, a circulation pump is required to circulate the solution.

While the COP of this cycle is not impressive compared to the vapor compression cycle, it can be driven mainly by waste heat instead of electricity, which is why it is used primarily in industrial applications.

The cycle described above is known as the single-effect cycle. There are more advanced cycles than single-effect (see the review of absorption technologies in [1]) and different types of absorbent-refrigerant mixtures; motivated by the practical study conducted in the sequel, however, this paper focuses on single-effect absorption cycles with Lithium-Bromide (LiBr) as absorbent and water as the refrigerant.

Control is highly important to effective operation of an absorption heat pump. First of all, the cycle needs to be kept stable; without measurement feedback, it may happen that the entire amount of absorbent gathers in either the absorber or the generator, causing the process to halt. Furthermore, the absorbent may crystallize if the pressure and temperature cross certain thresholds, and there are of course lifetime and optimality considerations as well. It is thus slightly surprising that while there are many references on modeling of absorption heat pumps—see e.g., [1], [2], [3], [4], [5], [6], [7]—the literature on control is rather sparse. [8] mentions the addition of motor valves instead of throttle valves for improved control. [9] and [10] discuss control strategies to avoid crystallization. [11] discusses generator level control using the solution circulation pump as actuator. [12] presents a robust control design using the solution pump to control system capacity. [13] discusses external water flow control, which can be considered as taking an input/output view of the absorption heat pump process.

However, it appears that no analysis of potential control configurations for absorption heat pumps have been reported in literature. In this paper, we use the so-called Relative Gain Array (RGA) analysis ([14], [15]) to investigate the best input/output pairings for control of a generic heat pump model derived in a companion paper [16]. The analysis is carried out on a simulation model of an actual industrial absorption heat pump situated at Sønderborg Fjernvarme (SFJV); a district heating plant in the southern part of Denmark. Simulations with the control configuration suggested by the RGA analysis, indicate that some performance increase can be expected by reconfiguring the control system.

The rest of the paper is organized as follows. In Section II, we briefly describe the nonlinear model of the absorption heat pump. Then, in Section III we briefly recount the RGA method. Section IV discusses candidate outputs, while Section V presents the results of the analysis. Section VI shows some illustrative simulations. Finally, Section VII gives concluding remarks.

*This work was financially supported by the Danish Energy Agency through the EUDP project GreenFlex (jn:64013-0133) and the Faculty of Engineering and Science at Aalborg University

[1]K. Vinther, K. Nielsen, P. Andersen, T. Pedersen and J. Bendtsen are with the Section of Automation and Control, Department of Electronic Systems, Aalborg University, 9220 Aalborg, Denmark {kv,kmn,pa,tom,dimon}@es.aau.dk

[2]R. Nielsen is with Added Values, 7100 Vejle, Denmark RJN@AddedValues.eu

II. Model Description

A single-effect LiBr-water absorption cycle is illustrated in Fig. 1. The cycle consist of four main components: an evaporator, an absorber, a generator, and a condenser. Thermodynamic state points are numbered in the figure (adopted from [13], [17]) and characterize the properties of the internal state of a liquid LiBr-water solution (1-6), water vapor (7, 10), and liquid water (8, 9) and the external state of a hot water source (11, 12), cooling water (13-16) and chilled water (17, 18). Further, two valves and a solution pump provide the required circulation of solution and refrigerant internally in the absorption cycle. Depending on the setup, some systems also have an additional solution heat exchanger (HEX) and a water HEX (19, 20) for improved efficiency.

The dynamic model of the absorption cycle used in this work is based on mass and energy balances, and thermodynamic property functions. It is assumed that the evaporator and absorber operate at the same low pressure, and that the generator and condenser operate at the same high pressure. Further, there are no heat losses to the ambient air and each of the four main components can be represented by a liquid control volume (subscript l) and a vapor control volume (subscript v). The overall mass balances are

$$\text{Eva:}\quad \frac{dM_e}{dt} = m_9 - m_{10}, \tag{1}$$

$$\text{Abs:}\quad \frac{dM_a}{dt} = m_6 + m_{10} - m_1, \tag{2}$$

$$\text{Gen:}\quad \frac{dM_g}{dt} = m_3 - m_4 - m_7, \tag{3}$$

$$\text{Con:}\quad \frac{dM_c}{dt} = m_7 - m_8, \tag{4}$$

$$\begin{aligned} M_i &= V_{i,l}\rho_{i,l} + V_{i,v}\rho_{i,v} \\ &= V_{i,l}\rho_{i,l} + (V_{i,tot} - V_{i,l})\rho_{i,v} \end{aligned} \tag{5}$$

where M is mass, V is volume, ρ is density, m correspond to mass flows illustrated with arrows in Fig. 1, $i \in \{e, a, g, c\}$ in (5) and (12) denote each component, and subscript tot denotes total. The LiBr mass balances are

$$\text{Abs:}\quad \frac{d\left(X_a V_{a,l}\rho_{a,l}\right)}{dt} = X_6 m_6 - X_1 m_1, \tag{6}$$

$$\text{Gen:}\quad \frac{d\left(X_g V_{g,l}\rho_{g,l}\right)}{dt} = X_3 m_3 - X_4 m_4, \tag{7}$$

where X is mass fraction of LiBr. The energy balances are

$$\text{Eva:}\quad \frac{dU_e}{dt} = m_9 h_9 - m_{10} h_{10} + Q_e, \tag{8}$$

$$\text{Abs:}\quad \frac{dU_a}{dt} = m_6 h_6 + m_{10} h_{10} - m_1 h_1 - Q_a, \tag{9}$$

$$\text{Gen:}\quad \frac{dU_g}{dt} = m_3 h_3 - m_4 h_4 - m_7 h_7 + Q_g, \tag{10}$$

$$\text{Con:}\quad \frac{dU_c}{dt} = m_7 h_7 - m_8 h_8 - Q_c, \tag{11}$$

$$U_i = V_{i,l}\rho_{i,l}h_{i,l} + V_{i,v}\rho_{i,v}h_{i,v} - p_i V_{i,tot} \tag{12}$$

where U is internal energy, Q is heat transfer rate, h is specific enthalpy, and p is pressure. The mass and energy balances are supplemented with thermodynamic property functions (e.g., to calculate enthalpy and density). The water property functions are part of the standard *Modelica* Media library and the LiBr-water solution property functions are implemented based on the formulations given in [18]. It is further assumed (see also [17]) that the solution that exits the absorber and generator, the water that exits the condenser, and the vapor that exits the evaporator, all are in a saturated state (same state as in the respective components).

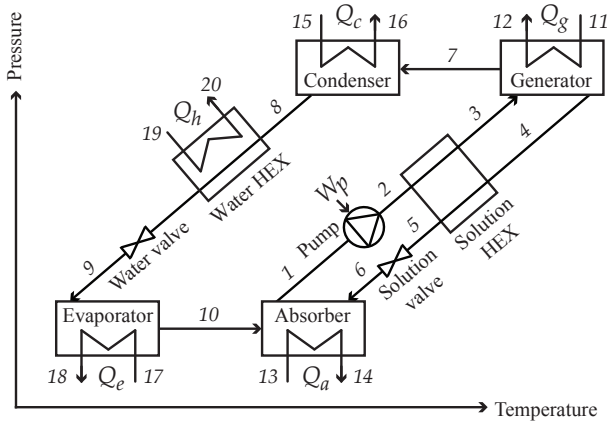

Fig. 1. Single-effect LiBr-water absorption heat pump cycle model. The numbers indicate state points used in the model.

The six HEX illustrated in Fig. 1 are modeled using 1-dimensional dynamic staggered grid flow models with a finite volume model representation with N discrete volumes (volume divided equally). The energy balance equation for the j'th volume, $j = 1, \ldots, N$, is;

$$\frac{d\left(\frac{V_{tot}}{N}\rho_j h_j - p_j \frac{V_{tot}}{N}\right)}{dt} = m_{j-1}h_{j-1} - m_j h_j + Q_{wall,j}, \tag{13}$$

$$Q_{wall,j} = \frac{UA}{N}(T_{wall,j} - T_j), \tag{14}$$

$$UA = UA_{no}\left(\frac{|m_j|}{m_{no}}\right)^{0.8}, \tag{15}$$

where UA is a mass flow dependent overall heat transfer coefficient, subscript $_{no}$ defines nominal values, and T_{wall} is pipe wall temperature. Inlet and outlet pressure are assumed equal for each volume and the outlet temperature of each volume is equal to the temperature of that volume T_j. Furthermore, the pipe wall temperature is modeled by

$$\frac{M_{wall}}{N} c_{p,wall} \frac{dT_{wall,j}}{dt} = Q_{wall,in,j} - Q_{wall,out,j}, \tag{16}$$

where $Q_{wall,in}$ and $Q_{wall,out}$ are the heat transfer rate into and out of the wall, respectively, and $c_{p,wall}$ is the specific heat capacity of the wall material. To keep the model simple, the water heat exchangers for the four main components are assumed to have saturation temperature along the entire length of the secondary side of the wall (internal heat pump temperature). The pressure drop Δp_j across the j'th flow element, $j = 1, \ldots, N+1$, located between the N volume

elements in the staggered grid models, is calculated as

$$\Delta p_j = \frac{K_f}{\rho_j} m_j |m_j|, \tag{17}$$

where K_f is a fixed flow coefficient for each flow element. Note that the pressure loss internally in the heat pump cycle, between state points 2-3, 4-5, and 8 to before the water valve, are assumed to be negligible and thus set to zero (together with static mass balances). This reduces model complexity considerably and improves simulation speed.

A linear static equation is used to describe the mass flow rate through the valves;

$$K_v m_v = \alpha \Delta p_v, \tag{18}$$

where K_v is a fixed flow coefficient, m_v is mass flow through the valve, α is valve opening degree, and Δp_v is the differential pressure across the valve. Finally, the mass flow through the solution pump m_1 is related to the pump work W_p via the static equation

$$\eta_p W_p = \Delta p_p \frac{m_1}{\rho_p}, \tag{19}$$

where η_p is a fixed pump efficiency and ρ_p is the density of the incompressible solution.

An implementation of the above model in *Dymola* using the *Modelica* modeling language has been compared with data from a single-effect LiBr-water absorption cycle heat pump located at SFJV. The heat pump is from Hope Deepblue Air-conditioner Manufacture Corp., Ltd., has model number RXZ698, and has an operational weight of 67 ton [19]. The comparison is shown in Fig. 2. For further detail on the heat pump and additional comparison of data see [16]. Note that the comparison is made with internal feedback control of generator concentration (controlled by the solution pump), generator and condenser levels (controlled by the valves), and condenser temperature (controlled by the external generator water mass flow) in order to stabilize the system (control setups will be further discussed in subsequent sections). The exact feedback loops at SFJV are unknown and also include various logic/algorithms, e.g., for determination of the setpoint for concentration and pressure/temperature and safety dilution procedures. However, only the stabilizing feedback loops are investigated here.

The top plot in Fig. 2 shows the external water mass flows measured during a 20 hour period at SFJV. These mass flows and the inlet water temperatures for the evaporator, absorber, generator, and condenser have been used as input data to the simulation. Notice that the system first operates at a low flow situation and then ramps up to a higher capacity situation. The evaporator and condenser pressures show good agreement between real data and simulation. The temperature increase across the four main water heat exchangers also show reasonable results, with the largest deviation in the absorber, where the error is flow dependent. Improvement of the model is not the focus of this paper and it is considered adequate for analysis of control structures.

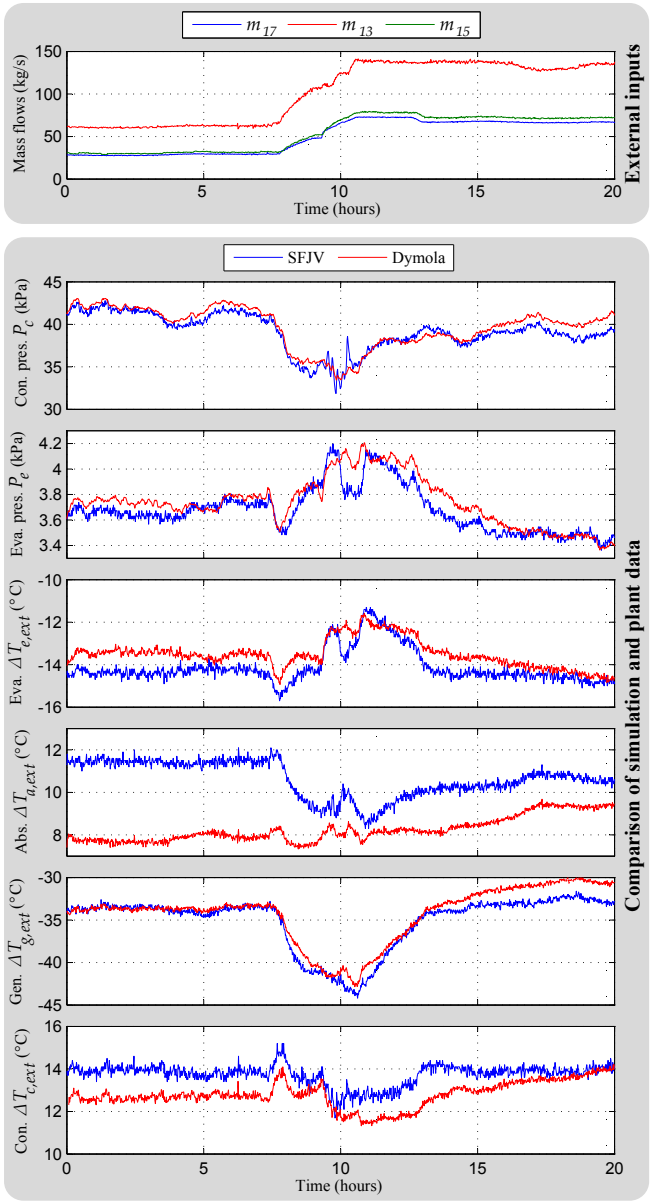

Fig. 2. Comparison of data from SFJV and *Dymola* simulation. The mass flows and the increase in temperature of the external water flow are shown for the four main components.

III. Relative Gain Array Analysis

The relative gain array (RGA) and the condition number are two measures, which can be used to evaluate the degree of directionality, potential controllability problems, and the level of interactions in MIMO systems. They can therefore be used to help to design a decentralized controller and to pair controllable inputs with system outputs. This section gives a summary of the important properties of the two measures and is based on more detailed discussions provided in [14].

Let $G(s) \in \mathbb{C}^{p \times p}$ be the transfer function matrix of a system to be evaluated. The *RGA matrix* for the system evaluated at some frequency $\omega \in \mathbb{R}_+ \cup \{0\}$ is defined as

$$R(G(j\omega)) = G(j\omega) \times (G(j\omega)^{-1})^T, \tag{20}$$

where $\times$ denotes element-by-element multiplication. Each element in the RGA matrix is a measure of interaction between the corresponding input-output pair. Note that it is independent of input and output scaling. The following two pairing rules can be used for design of decentralized control:

- PR1: Prefer to pair input and outputs that have RGA elements close to 1 at frequencies around the closed-loop bandwidth.
- PR2: Pairing of negative steady-state RGA elements should be avoided if possible.

The intention behind the first pairing rule is that an RGA element close to 1 at all frequencies means that the gain of this input-output pairing is unaffected by closing the other loops, which is desirable. Since the RGA matrix is frequency dependent, the most interesting frequency is around the closed-loop bandwidth. Additionally, large RGA elements (5-10 or larger) is an indication of fundamental control difficulties due to sensitivity to uncertainty and strong interactions in the system (cross-couplings). PR2 is related to *decentralized integral controllability* (DIC). In short, if a system satisfy DIC then there exists a stabilizing decentralized controller with integral action in each loop, where each loop can be (de-)tuned independently without introducing instability. A system only has DIC if pairing of negative steady-state RGA elements is avoided. One should thus avoid pairings corresponding to negative steady-state RGA elements in order to maintain integrity of the closed-loop system (e.g., if a subsystem controller is brought out of service, detuned, or if the input saturates). Another important check is to see if the RGA elements corresponding to the chosen pairing changes sign with frequency, since this implies the presence of right half plane zeros, which degrade potential performance of the closed-loop control. Finally, it is favorable to pair inputs and outputs close to each other in terms of effective delay, since this can be a limiting factor for high-gain feedback.

Determining the appropriate pairing according to rule 1 and 2 can sometimes be difficult for large matrices. A simple selection measure is the *RGA number* $R_E(G((j\omega_{cbw})))$ computed at the closed-loop bandwidth ω_{cbw}:

$$R_E(G(j\omega_{cbw})) = ||R(G(j\omega_{cbw})) - E||_{\sum}, \qquad (21)$$

where $||A||_{\sum} = \sum_{i,j} |a_{ij}|$ is the sum norm and $E \in \mathbb{R}^{p\times p}$ is a permutation matrix representing the pairing in question (e.g., $E = I$ for a diagonal pairing). In general, R_E should be small. However, the pairing corresponding to the smallest number does not guarantee diagonal dominance of the rearranged system. Another useful measure is an iterative evaluation of RGA defined as

$$R_\infty(G(j\omega_{cbw})) = \lim_{k\to\infty} R^k(G(j\omega_{cbw})), \qquad (22)$$

since this always converges to an identity matrix if G is a generalized diagonally dominant matrix (usually it is enough to make 4-8 iterations). A disadvantage of the iterative RGA is that it might suggest negative pairings.

The RGA matrix can also be computed for non-square matrices using the pseudo-inverse, which can be used as a tool to select appropriate input/output sets for pairing analysis. If there are more inputs than outputs and the element sum of a column is small then the corresponding input could be deleted as it does not really affect the outputs. The same goes for a situation with more outputs than inputs, where the row sum should not be too small. For more detail on non-square RGA analysis see, e.g., [15]. Another measure that can help in the selection of a set of outputs to control, when there are more potential outputs than inputs, is the condition number, which is defined as

$$\gamma(G(j\omega)) = \frac{\overline{\sigma}(G(j\omega))}{\underline{\sigma}(G(j\omega))}, \qquad (23)$$

where $\overline{\sigma}$ and $\underline{\sigma}$ are the largest and smallest singular values of G at the frequency ω. It is then desirable to choose the output set that gives the smallest condition number, as a large number may indicate control difficulties. However, the condition number is not independent of input and output scaling. Scaling of $G \in \mathbb{C}^{p\times m}$ is therefore necessary, leading to a scaled condition number γ^* defined as

$$\gamma^*(j\omega) \equiv \gamma(D_y G(j\omega) D_u) = \frac{\overline{\sigma}(D_y G(j\omega) D_u)}{\underline{\sigma}(D_y G(j\omega) D_u)}, \qquad (24)$$

where $D_u \in \mathbb{R}^{m\times m}$ and $D_y \in \mathbb{R}^{p\times p}$ are diagonal input and output scaling matrices, respectively. These scaling matrices can be based on the largest expected or desired values of the inputs and outputs. In this paper we will choose the input scaling with respect to the expected input variation (limited due to constraints) and the output scaling with respect to the maximum desired tracking error.

IV. Output Selection

Inputs and potential output to be controlled are first identified before these are paired. The analysis is based on the heat pump setup at SFJV, which is illustrated in Fig. 1.

The external water mass flows are controlled in the following way: The evaporator mass flow m_{17} is first set based on a desired capacity utilization of the heat pump (operating condition of interest). The absorber mass flow m_{13} is then set to $1.591m_{17}$ or within 95 to 160% of that value and the condenser mass flow m_{15} is likewise a scaling of the evaporator flow and set to $1.078m_{17}$ or within 85 to 115% of that value. The chosen scalings and intervals are determined by the specifications from the heat pump manufacturer. The mass flow through the water HEX is also scaled according to evaporator flow with $m_{19} = 0.0266m_{17}$. Alternatively, m_{19} can be controlled to give a fixed outlet temperature at state point 20. Note that the output selection and pairing analysis is based on the transfer function matrix G, defined in Section III, and G will in general be affected by the choice of operating conditions.

The remaining inputs are generator mass flow m_{11}, solution valve opening degree α_s, water valve opening degree α_w, and pump mass flow m_1. The focus in this paper is to pair these four inputs with suitable outputs, in order to stabilize the system when the capacity is changed according to the described control of external water flows.

TABLE I

INPUTS AND OUTPUTS CONSIDERED IN THE PAIRING ANALYSIS.

Input	Output	Description	Range	Unit
m_{11}		Ext. gen. water mass flow	0-180	$\frac{kg}{s}$
α_s		Solution valve opening degree	0-100	%
α_w		Water valve opening degree	0-100	%
m_1		Solution pump mass flow	0-30	$\frac{kg}{s}$
	L_e	Eva. liquid level	0-100	%
	L_a	Abs. liquid level	0-100	%
	L_g	Gen. liquid level	0-100	%
	L_c	Con. liquid level	0-100	%
	X_4	Gen. LiBr mass fraction	0-100	%
	T_e	Eva. temperature	>273.15	K
	T_g	Gen. temperature	$> T_c$	K
	T_c	Con. temperature	$> T_e$	K

The available heat pump output measurements, based on the setup at SFJV, are generator level L_g (here levels are determined as volume of liquid relative to total volume in per cent), generator outlet concentration X_4, temperature of liquid water in the evaporator T_e, generator solution temperature T_g, and temperature of water out of the condenser T_c. In addition, the three levels L_e, L_a, and L_c are added as outputs to analyze their potential use.

The inputs and outputs are summarized in Table I. The external generator and the solution pump mass flow are controlled directly, but these inputs could as well have been valve opening degree and pump frequency. The input scaling D_u in Eq. (24) is based on the minimum expected available range due to constraints; 15 kg/s in generator mass flow, 10% in valve opening degree, and 5 kg/s in pump mass flow.

Some systems have an overflow u-tube design with condenser and generator elevated above evaporator and absorber instead of valves from condenser to evaporator and from generator to absorber. In the following it is assumed that these valves are electronic expansion devices with variable opening degree, which provides two additional degrees of freedom. In section VI, the potential performance of a four input setup with a two input setup using the u-tube design is compared. The u-tube design is emulated with the valve models by opening the valves when the levels exceed an upper threshold value (overflow), e.g. 0% open when level is below the threshold and gradually increased to 100% when the level is 0.1% above the threshold.

The pairing analysis requires the transfer function matrix $G(s)$ between the inputs and the potential outputs. An alternative, if this model is not available or if the system is considered as a black box, is to perturb each input individually with a sinusoidal signal and identify the resulting perturbation in each output to get the frequency response of G. This should then be repeated for the frequencies of interest. The input perturbation should be applied in open loop. An initial stabilizing control setup is therefore required in order to bring the system to steady state first. The frequency response result of such an alternative non model-based procedure is used in this paper and shows good agreement with $G(s)$ obtained using *Dymola*'s linearize functionality on the full nonlinear model, see [16]. Additionally, if the amplitude of the sinusoidal perturbation is close to the amplitude of the control signals applied later in closed loop, then more of the effect of the nonlinearities will be included in the input/output pairing analysis.

The frequencies of interest should be centered around the desired closed-loop bandwidth ω_{cbw}. This bandwidth can be determined based on the maximum allowed rate of change of the main disturbance input, which is the evaporator mass flow with a limit of 168 kg/s/hour. This disturbance should not affect the eight outputs more than a design specification; 1 percentage point in concentration, 10% in levels (relative to reference level), and 2 degrees in temperature. These values are also used as output scaling D_y in Eq. (24) and as performance measure in Section VI. By perturbing the evaporator mass flow in open loop with a sinusoidal signal with a period of 45 minutes and an amplitude $A = 21.5$ kg/s (based on the rate of change limit and the minimum and maximum evaporator flows shown in Fig. 2), it is possible to get an approximation of the required damping of the control and the corresponding closed-loop bandwidth. Further, to account for uncertainties a factor two in frequency is used. This gives a desired bandwidth between $0.0033 - 0.0091$ rad/s depending on the output (0.0091 is used in the following).

Fig. 3 shows the frequency dependent non-square RGA row sums corresponding to each of the eight outputs in the system. None of the row sums are significantly below 1, which indicates that they are all potential candidates for control by the four chosen inputs. Note that the total sum of the row sums is equal to the dimension of G and that at most four outputs can be kept under perfect control with decentralized control (there are four inputs). Further, choosing the outputs with the highest row sums does not necessarily give the best performance [15]. Multiple pairings should therefore be checked before a conclusion is made.

Keeping the right LiBr concentration out of the generator is important, since the solution returning to the absorber is closest to the crystallization limit. The output X_4 is therefore chosen in all setups. Maintaining levels and thus the correct distribution of refrigerant and solution in the evaporator, absorber, generator, and condenser is important for continued stable operation of the cycle. The levels are integrator

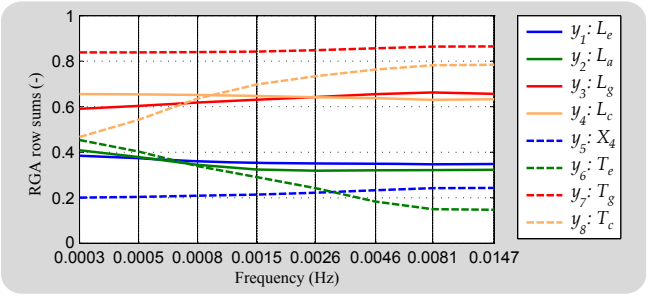

Fig. 3. RGA row sums and their corresponding outputs.

systems and inherently unstable without proper control of internal flows between components. However, precise level measurements are difficult to obtain and expensive to install. Additionally, control of four levels is difficult as they are not independent variables in the closed heat pump system. Control of three temperatures and no levels can similarly not be performed independently (T_c and T_g are both directly related to the same pressure), which leaves combinations of three, two, and one level measurements to be analyzed in the following.

V. Analysis of Candidate Input/Output Pairings

Table II shows the suggested pairings based on iterative RGA, the diagonal of the RGA matrix *diag*(R), the RGA number R_E, and the scaled condition number γ^*, at the desired closed loop bandwidth ω_{cbw}, for six selected input-output sets. None of the presented setups have negative pairings (pairing rule PR2). Setup no. 7 shows the chosen input-output pairing in an alternative two input two output system without controllable valves (u-tube overflow setup).

Setups no. 1 and 2 are the recommended three level alternatives with decent and almost equivalent numbers. The two other three level alternatives L_g, L_a, L_c and L_g, L_a, L_e should potentially be better, since respective inputs and outputs are physically located closer to each other (m_{11} controls L_g instead of L_c). However, the numbers are worse and it is difficult, if not impossible, to avoid negative pairings.

Setups no. 3 and 4 are the recommended two level alternatives. The best numbers are obtained using T_c instead of T_g or T_e. This is because the condenser saturation temperature T_c is directly related to pressure and m_{11} (amount of steam generated), whereas the generator temperature T_g is also a function of the concentration (e.g., compare numbers in Setup no. 3 with Setup no. 5). The evaporator saturation temperature T_e is more difficult to control, as it is located far from potential inputs except α_w, but this input should control either L_e or L_c. The other combinations of level measurements also produce worse numbers and a requirement is that at least L_g or L_a should be measured together with X_4 to maintain a suitable LiBr mass distribution in the system. The two input Setup no. 7 is similar to Setup no. 3 if it only has overflow level control; no. 7 is the setup used in the model verification presented in Section II and is believed to be close to the setup used in the heat pump at SFJV.

The one level setup no. 6 has the best numbers. However, despite that the pairing has high potential in terms of regulating the chosen outputs to a desired reference (temperatures are easier to control than levels), feedback on one level is not enough to maintain all four levels within their requirements; this setup is thus not recommended.

VI. Verification of Control Setup

Closed-loop simulations of Setups no. 1, 3, and 7 are presented in Fig. 4. The results show that they all maintain stable operation under step changes in capacity. Simple decentralized control in terms of PI feedback loops have been applied to each input-output pair and manually tuned to keep the output within the performance specification outlined in Section IV. The external inputs in the simulation are all the external water inlet temperatures and the evaporator mass flow. These inputs are real data from operation of the heat pump at SFJV. A step up and a step down is added to the evaporator mass flow data and scaling of this mass flow gives the absorber, condenser, and water HEX mass flows. Note that step changes in evaporator mass flow is not allowed on the real system (rate limitation of 168 kg/s/hour), but applied here to test the control loops.

Setup no. 3 cannot keep the two uncontrolled levels L_e and L_a at the setpoint. However, they are within the performance bound and stay stable also for longer simulations. Two controlled levels, generator concentration, and condenser temperature/pressure is enough to keep the cycle stable and a suitable distribution of mass between the four main components. The two input Setup no. 7 has similar performance as Setup no. 3, except for a slightly higher level in the generator and condenser due to the overflow mechanisms. A benefit of the four input system is that the heat pump can be operated at different level setpoints giving more freedom in choosing operating conditions. The four input setup also puts less requirements on mechanical design (u-tubes and elevation of components). However, more actuators and sensors are required. The benefit of having three level sensors in Setup 1 seems small, since keeping the condenser temperature/pressure at a given setpoint might be more important than keeping all levels at their exact setpoints.

An extension of the results could be to design decoupling

TABLE II

Comparison of candidate input-output pairings with suggested pairings column based on Eq. (22). The recommended pairings are indicated with a bold number (two and a three level alternatives). Pairing 7 is a setup with only two controllable inputs and overflow mechanisms in the condenser and generator.

No.	Suggested pairing	*diag*(R)	R_E	γ^*
1	$m_{11} \rightarrow L_c$ $\alpha_s \rightarrow L_g$ $\alpha_w \rightarrow L_e$ $m_1 \rightarrow X_4$	$0.80-0.014j$ $1.15-0.89j$ $0.85-0.11j$ $1.34-0.80j$	5.36	23.04
2	$m_{11} \rightarrow L_g$ $\alpha_s \rightarrow L_a$ $\alpha_w \rightarrow L_e$ $m_1 \rightarrow X_4$	$0.81-0.069j$ $1.10-0.96j$ $0.86-0.15j$ $1.34-0.79j$	5.50	23.22
3	$m_{11} \rightarrow T_c$ $\alpha_s \rightarrow L_g$ $\alpha_w \rightarrow L_c$ $m_1 \rightarrow X_4$	$0.93+0.011j$ $1.24-0.58j$ $1+0.0020j$ $1.23-0.43j$	2.98	8.20
4	$m_{11} \rightarrow T_c$ $\alpha_s \rightarrow L_a$ $\alpha_w \rightarrow L_e$ $m_1 \rightarrow X_4$	$0.92+0.010j$ $1.22-0.56j$ $1+0.0030j$ $1.24-0.40j$	2.90	10.00
5	$m_{11} \rightarrow T_g$ $\alpha_s \rightarrow L_g$ $\alpha_w \rightarrow L_c$ $m_1 \rightarrow X_4$	$1.34-0.40j$ $1.24-0.58j$ $1+0.0020j$ $1.55-1.20j$	5.44	11.34
6	$m_{11} \rightarrow T_c$ $\alpha_s \rightarrow T_e$ $\alpha_w \rightarrow L_c$ $m_1 \rightarrow X_4$	$1.01+0.14j$ $0.94-0.22j$ $1+0.0031j$ $0.88-0.086j$	1.39	5.15
7	$m_{11} \rightarrow T_c$ $m_1 \rightarrow X_4$	-	-	-

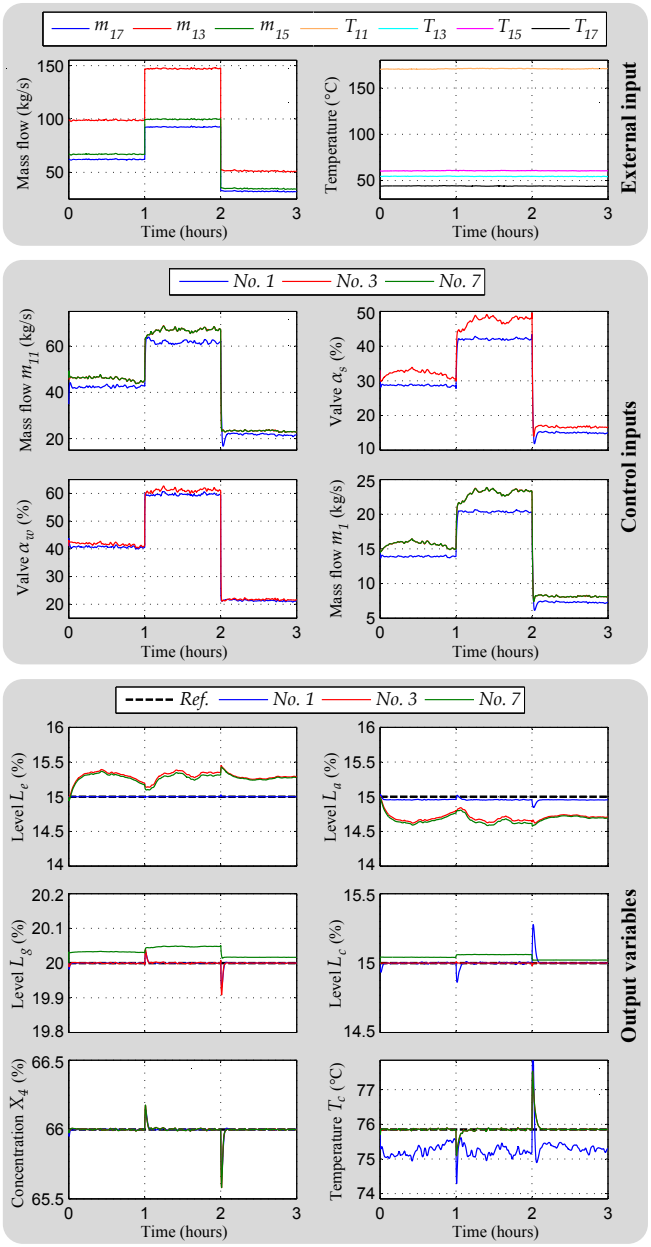

Fig. 4. Closed-loop simulation results during steps in external mass flows with control Setup no. 1, 3, and 7.

or MIMO controllers, e.g. LQ control, for the selected setups to better handle cross couplings. Further, the analysis presented in this paper has been performed using frequency responses obtained in a typical operating condition for the heat pump. However, a verification of the analysis could be performed in other operating points as well.

VII. Conclusion

A dynamic nonlinear model of an absorption heat pump has been presented. This model can be used as a benchmark for control design and by conducting open-loop tests it is possible to identify the frequency response from potential inputs to potential outputs. This information can be used to compute a non-square RGA matrix for output selection and feasible sets of four inputs and four outputs (out of eight) were identified. Analysis using RGA calculation and condition numbers can then be used to chose the best pairings in these sets and to find a suitable decentralized control structure, which is often favored by industry. Results in this paper have shown that in the case with four decentralized controllers at least two and at maximum three of them should control levels in one of the four main components. Control of LiBr concentration is also important to avoid crystallization and simulation results have shown that selected control structures can give stable operation of the heat pump. The output selection and pairing suggestions in this paper could also be used to design more advanced control.

References

[1] P. Srikhirin, S. Aphornratana, and S. Chungpaibulpatana, "A review of absorption refrigeration technologies," *Renewable Sustainable Energy Rev.*, vol. 5, no. 4, pp. 343–372, 2001.

[2] S. Jeong, B. Kang, and S. Karng, "Dynamic Simulation of an Absorption Heat Pump for Recovering Low Grade Waste Heat," *Appl. Therm. Eng.*, vol. 18, no. 1-2, pp. 1–12, 1998.

[3] D. G. Fu, G. Poncia, and Z. Lu, "Implementation of an object-oriented dynamic modeling library for absorption refrigeration systems," *Appl. Therm. Eng.*, vol. 26, no. 2-3, pp. 217–225, 2006.

[4] Y. Shin, J. A. Seo, H. W. Cho, S. C. Nam, and J. H. Jeong, "Simulation of dynamics and control of a double-effect LiBr-H2O absorption chiller," *Appl. Therm. Eng.*, vol. 29, no. 13, pp. 2718–2725, 2009.

[5] J. Sun, lin Fu, S. Zhang, and W. Hou, "A mathematical model with experiments of single effect absorption heat pump using LiBr-H2O," *Appl. Therm. Eng.*, vol. 30, no. 17-18, pp. 2753–2762, 2010.

[6] M. Chamoun, R. Rulliere, P. Haberschill, and J. F. Berail, "Dynamic model of an industrial heat pump using water as refrigerant," *Int. J. Refrig.*, vol. 35, no. 4, pp. 1080–1091, 2012.

[7] A. Iranmanesh and M. Mehrabian, "Dynamic simulation of a single-effect LiBr-H2O absorption refrigeration cycle considering the effect of thermal masses," *Energy Build.*, vol. 60, pp. 47–59, 2013.

[8] D. Butz and K. Stephan, "Dynamic behavior of an absorption heat pump," *Int. J. Refrig.*, vol. 12, no. 4, pp. 204–212, 1989.

[9] K. Wang, O. Abdelaziz, P. Kisari, and E. A. Vineyard, "State-of-the-art review on crystallization control technologies for water/LiBr absorption heat pumps," *Int. J. Refrig.*, vol. 34, no. 6, pp. 1325–1337, 2011.

[10] X. Liao and R. Radermacher, "Absorption chiller crystallization control strategies for integrated cooling heating and power systems," *Int. J. Refrig.*, vol. 30, no. 5, pp. 904–911, 2007.

[11] J. A. Seo, Y. Shin, and J. D. Chung, "Dynamics and control of solution levels in a high temperature generator for an absorption chiller," *Int. J. Refrig.*, vol. 35, no. 4, pp. 1123–1129, 2012.

[12] A. Ohgata, Y. Yamashita, and H. Nishitani, "Robust control of An Absorption Heat Pump System," *Comput. Chem. Eng.*, vol. 21, pp. 131–136, 1997.

[13] P. Kohlenbach and F. Ziegler, "A dynamic simulation model for transient absorption chiller performance. part i: The model," *Int. J. Refrig.*, vol. 31, no. 2, pp. 217–225, 2008.

[14] S. Skogestad and I. Postlethwaite, *Multivariable Feedback Control - Analysis and Design*, 2nd ed. John Wiley & Sons, Ltd, 2005.

[15] J. wen Chang and C. ching Yu, "The Relative Gain for Non-square Multivariable Systems," *Chem. Eng. Sci.*, vol. 45, no. 5, pp. 1309–1323, 1990.

[16] K. Vinther, R. J. Nielsen, K. M. Nielsen, P. Andersen, T. S. Pedersen, and J. D. Bendtsen, "Absorption Cycle Heat Pump Model for Control Design," in *ECC*, Linz, Austria, July 2015, in press.

[17] K. E. Herold, R. Radermacher, and S. A. Klein, *Absorption Chillers and Heat Pumps*. CRC Press, 1996.

[18] J. Pátek and J. Klomfar, "A computationally effective formulation of the thermodynamic properties of LiBrH2O solutions from 273 to 500K over full composition range," *Int. J. Refrig.*, vol. 29, no. 4, pp. 566–578, 2006.

[19] Hope Deepblue Air Conditioning Manufacture Corp., Ltd. (2014, Sep.) Hot water-type libr absorption chiller. [Online]. Available: http://www.slhvac.com/productsinfo.aspx?NId=8&NodeID=15